Experimental and theoretical study of the Kr *L*-shell Auger decay

N. Boudjemia,[1] K. Jänkälä,[1] T. Gejo,[2,3] Y. Kohmura,[2] M. Huttula,[1] M. N. Piancastelli,[4,5,2] M. Simon ●,[4,2] M. Oura ●,[2] and R. Püttner ●[6]

[1]*Nano and Molecular Systems Research Unit, University of Oulu, P.O. Box 3000, 90014 Oulu, Finland*
[2]*RIKEN SPring-8 Center, 1-1-1 Kouto, Sayo-cho, Sayo-gun, Hyogo 679-5148, Japan*
[3]*Graduate School of Materials Science, University of Hyogo, Kamigori-cho, Ako-gun, Hyogo 678-1297, Japan*
[4]*Sorbonne Université, CNRS, Laboratoire de Chimie Physique-Matière et Rayonnement, LCPMR, F-75005 Paris Cedex 05, France*
[5]*Department of Physics and Astronomy, Uppsala University, SE-75120 Uppsala, Sweden*
[6]*Fachbereich Physik, Freie Universität Berlin, Arnimallee 14, D-14195 Berlin, Germany*

The *LMM* Auger spectra of krypton are measured using the photon energies $h\nu = 1709$ eV, 1792 eV, 1950 eV, and 13 keV. This approach allows separating the contributions from the various core holes L_1, L_2, and L_3. Previously unobserved transitions are presented. Complementary theoretical work is performed allowing the assignment of the spectral features. The $L_{2,3}Y\text{-}MMY$ ($Y = M_{4,5}, N_{1,2,3}$) Auger transitions of Kr^{2+} formed via Coster-Kronig Auger decay of the core holes L_1 and L_2 are also investigated. These spectra comprise about 4000 and 13 000 transitions, respectively, so that only general statements on the assignment, such as the configurations involved in the transitions, can be given.

I. INTRODUCTION

In the last decade electron-spectroscopy studies of isolated atoms and molecules with hard x-ray radiation of several keV have attracted substantial attention. This attention is mainly due to significant development of instrumentation in this energy region, both for light sources and detectors, which is driven by hard x-ray photoelectron spectroscopy (HAXPES) for solid state physics and materials science, with the goal to study bulk properties and buried interfaces. This recent technical development allows also for dilute-matter high-resolution studies with excellent signal-to-noise ratio.

Using these new opportunities, many interesting effects have been observed in the last decade. These include the translational [1] and rotational Doppler [2] effect in atomic and molecular Auger spectra as well as the rotational recoil [3]. Using a photon energy of 40 keV Kircher *et al.* found that the photoelectron recoil influences the angular distribution of the N 1*s* photoelectrons of N_2 [4]. Another important field is the investigation of deep double core holes like Ar and Cl $1s^{-1}2p^{-1}$ [5,6] as well as Ne and S $1s^{-2}$ [7,8].

In the last few years also very deep core holes such as the *K* shells of Br [9], Kr [10], I [11], and Xe [12] became accessible for high-resolution spectroscopy. A recent review with more details on these topics has been published by Piancastelli *et al.* [13].

In addition to this variety of new and interesting effects, the recent instrumental improvements provide also an excellent opportunity to revisit fundamental processes such as Auger decays of deep core holes and study them in unforeseen detail. For example, recent studies of the *KLL* Auger spectra of atomic argon [14] and sulfur in H_2S [15] provided detailed information about the satellite structure. In particular, both studies demonstrated that shake processes during the Auger decay cannot be neglected although they were completely ignored in previous studies; note that for these studies tunable photon energies were very essential. In addition, for Ar $1s^{-1}3l^{-1}nl^1 \rightarrow 2p^{-2}(^1D_2, ^1S_0)$ Auger satellites were observed. A detailed investigation showed that these transitions can only be explained by the knock-down effect since an angular-momentum transfer between the outgoing Auger electron and the excited valence electron is required [14].

For krypton, three detailed studies [16–18] were performed in the 1970s and 1980s. These studies assigned the lines of the most intense groups of Auger transitions, namely $L_{2,3}M_{2,3}M_{2,3}$, $L_{2,3}M_{2,3}M_{4,5}$, and $L_{2,3}M_{4,5}M_{4,5}$. The work of Levin *et al.* [18] also reported the less intense $L_3M_1M_{2,3}$ Auger transitions as well as one group of the L_1 Auger transitions, namely $L_1M_{4,5}M_{4,5}$. However, a systematic study of the L_1 Auger spectrum has not been reported so far. At the beginning of this millennium Suzuki *et al.* [19] performed a synchrotron-radiation based study of the $L_{2,3}M_{2,3}M_{4,5}$ and $L_{2,3}M_{4,5}M_{4,5}$ Auger transitions. The energy positions derived in this study were similar to those obtained earlier while the observed intensity ratios revealed differences. Finally, the resonant Kr $2p^{-1}nl$ Auger spectra were studied by Nagaoka *et al.* and Okada *et al.* [20,21].

Recently, the Kr 1*s* decay cascade in the region of the *L*-shell Auger transitions of Kr^{1+} to Kr^{3+} has been investigated [10] by the present group of authors. This work compared the Auger spectra of the *L*-shell region measured with photon energies lower ($h\nu = 13$ keV) and higher ($h\nu = 16.5$ keV) than the Kr $1s^{-1}$ ionization energy. From this comparison detailed information about the different decay

pathways of the K-shell core hole was derived. However, no detailed assignment of the spectral features in this spectral region was presented.

Within the present work we focus on the decay of direct L-shell ionization and report Auger spectra recorded at four different photon energies between 1709 eV and 13 keV. The photon energies were selected such that one spectrum shows only L_3 Auger transitions, a second one only L_2 and L_3 Auger transitions, and two more L_1, L_2, and L_3 Auger transitions. Note that the photon energy of 13 keV is not sufficient for K-shell ionization so that decays of the corresponding Auger cascade, which are discussed in detail in Ref. [10], cannot contribute to the spectra shown in the present publication. The latter two show different percentages for the contribution of L_1 transitions, indicating they contribute significantly only well above the corresponding threshold. In the electron kinetic energy range between 1100 and 1800 eV the Auger spectrum subsequent to L_1 ionization can be separated into two contributions. The first contribution is the direct decay of the L_1 core hole in Kr$^+$ via L_1XX ($X = M_{1,2,3,4,5}, N_{1,2,3}$) Auger decay. The second contribution dominates the spectrum and originates from a second-step Auger decay, namely the Auger decay of $2p^{-1}nl^{-1}$ states in Kr^{2+} which are formed via $L_1L_{2,3}Y$ ($Y = M_{4,5}, N_{1,2,3}$; i.e., contrary to X it does not include the deeper core holes $M_{1,2,3}$) Coster-Kronig decay of the initial L_1 core hole. The decay spectrum of the Kr$^{2+}(2p^{-1}nl^{-1})$ states consists of several thousand heavily overlapping lines so that they cannot be assigned individually. As a consequence, based on the present calculations we assign the visible spectral features only at the electron-configuration level. Moreover, general properties of the spectral features as obtained from the calculations will be discussed. Finally, additional details for less intense Auger groups of structures in Kr$^+$ could be observed, in particular in the pure L_3MM spectrum.

II. EXPERIMENTAL DETAILS AND THEORETICAL PROCEDURE

The experiments were carried out at the soft x-ray (SX) undulator beamline BL17SU and at the hard x-ray (HX) undulator beamline BL29XU of SPring-8, an 8 GeV synchrotron radiation facility in Japan.

As for the SX-energy region, a monochromatic photon beam in the 1709 to 1950 eV energy range was obtained using the grating monochromator [22–24] of beamline BL17SU. The resolving power of the photon beam, i.e., $\Delta E/E$, was set to be about 5.7×10^{-4} to achieve a higher photon flux; note that the resolving power has no influence on normal Auger spectra. The photon-beam size was about 0.2 (H) $\times$ 0.15 (V) mm^2 before introducing it into the apparatus. As for the HX-energy range, a Si(111) double-crystal monochromator, cooled by liquid nitrogen [25], of beamline BL29XU [26] was used to provide the 13 keV intense photon beam with the resolving power of about 1.33×10^{-4}. The photon beam was collimated to a size of 0.5×0.5 mm^2 at the upstream of the apparatus by using a four-jaw slit.

The apparatus equipped with the hemispherical electron energy analyzer SES-2002 and the gas-cell GC50 (ScientaOmicron [27]) was used for recording the Auger-

electron spectra. At beamline BL17SU, the apparatus was installed directly downstream of the exit slit of the beamline monochromator, and it was installed in the experimental hutch 3 (EH3) at BL29XU [28]. During the measurements, the target gas pressure was maintained to be about 1×10^{-3} Pa measured at the outside of the gas cell. The axis of the analyzer was in the horizontal direction at the right angle to the photon beam direction, i.e., parallel to the polarization vector of the incident photons. Note that L_3XX Auger spectra are generally not isotropic [29]. So, because of fixed non-magic-angle of measurements, the present data can be influenced by the non-isotropic angular distribution. However, it has been shown for Ar $2p_{3/2}^{-1}$ [30] and Xe $2p_{3/2}^{-1}$ ionization [31] that the alignment parameter $\mathcal{A}_{20}$ is small. We expect a similar small value for Kr $2p_{3/2}^{-1}$ ionization, resulting in only small angular-distribution effects, which do not influence the present results.

The energy resolution of the electron-energy analyzer was set to be 360 meV with a constant pass energy of 200 eV. The kinetic-energy scale of the electron spectrometer was calibrated by comparing the recorded Kr $M_{4,5}NN$ and Kr LMM Auger electron spectra with those reported in the literature [10,18,32].

The calculations were carried out using flexible atomic code (FAC) [33] which utilizes a fully relativistic approach based on configuration interaction Dirac-Fock theory. The atomic state functions (ASFs) with the total angular momentum J, its projection M, and parity P are constructed as linear combinations of configuration state functions (CSFs). The CSFs in their turn are antisymmetrized jj-coupled linear combinations of Slater determinants constructed as products of one-electron wave functions. The average level scheme is used in the optimization of one-electron wave functions and the mixing coefficients of the ASFs are solved by diagonalizing the electronic Hamiltonian. For precise prediction of the transition energies, Breit interactions and quantum electrodynamics (QED) corrections such as vacuum polarization and self-energy are included perturbatively to the final result. Those corrections are estimated to be tens of eV when dealing with core shells of atoms such as krypton [34].

The Kr$^+ \rightarrow$ Kr^{2+} Auger transitions in the kinetic energy range of 1000–1800 eV were calculated starting from the ionization of the Kr L shell, i.e., the Kr $L_{1,2,3}$ singly ionized states, in which all the possible final states are included, such as MM, MN, NN, and LM/LN induced via Coster-Kronig decay; the Coster-Kronig transitions to the latter final states can be found in the kinetic energy region of 4–223 eV and are not shown in the present work. For the second-step Auger decays in the studied energy region, the initial states LM and LN are taken for the calculation of the Kr$^{2+} \rightarrow$ Kr^{3+} Auger spectrum. In these calculations all the possible final states are also included. To obtain the correct widths of the Auger transitions, all the final states induced in the first- and the second-step Auger decay are assumed to undergo an additional Auger relaxation step.

The photoionization cross sections in dipole approximation at the selected photon energies and the Auger transition matrix elements were calculated using the standard formulations of the FAC code that provides the results in a non-time-consuming way due to the approximation of local potential and to the continuum wave function [33]. The transition
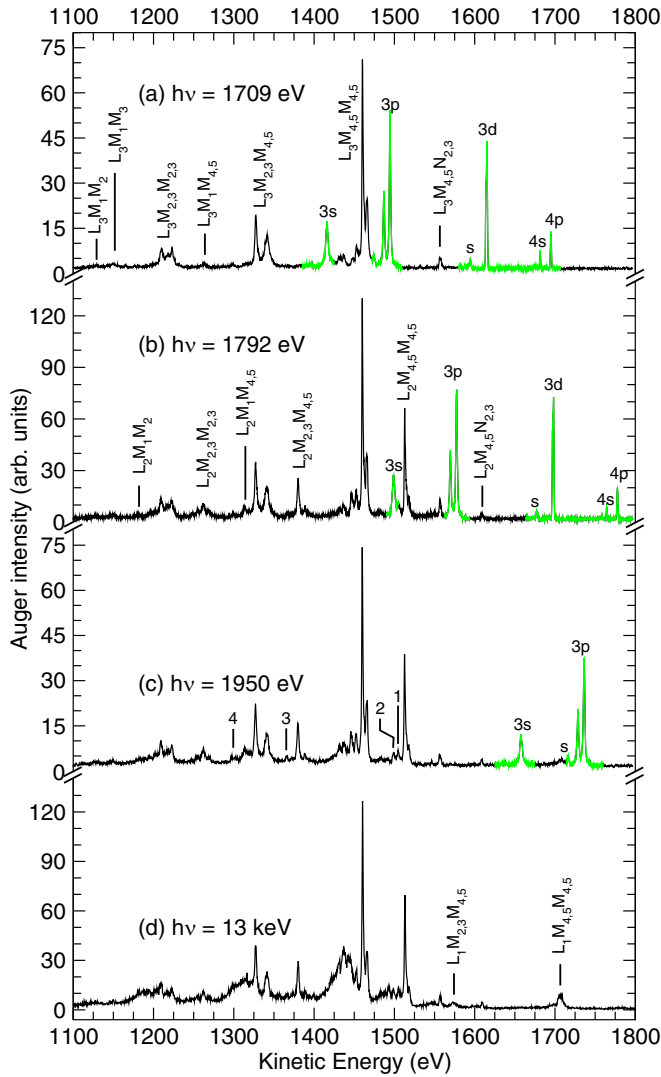
FIG. 1. Auger spectra in the energy range of 1100 to 1800 eV measured after ionization with photons of the energies (a) 1709 eV, (b) 1792 eV, (c) 1950 eV, and (d) 13 keV. Panel (a) shows the L_3-shell Auger decays and panel (b) the Auger decays of the L_2 as well as L_3 shells. Panels (c) and (d) show all three L-shell Auger decays. The structures indicated in green and labeled with nl are due to overlapping photoelectron lines. In panel (c) the vertical lines labeled with the numbers 1 to 4 indicate $L_2N_{1,2,3}$-$XXN_{1,2,3}$ Auger decays which are discussed in the text. For reasons of presentation the spectra in (a) and (c) are averaged over three data points.

amplitudes were calculated under Wentzel's ansatz [35,36], where both photoionization and Auger decay amplitudes are described by Fermi's golden rule. The calculations assume that the continuum electrons do not affect the final state bound orbitals, and higher order electron correlations such as postcollision interactions are neglected. The calculations, however, allow nonorthogonality between the initial and final state bound orbitals.

III. RESULTS AND DISCUSSION

Figure 1 shows the Auger spectra of Kr in the energy range of 1100 to 1800 eV measured after ionization with

TABLE I. Calculated relative cross sections for the orbitals Kr $2s$, Kr $2p_{1/2}$, and Kr $2p_{3/2}$ as a function of the photon energy.

Photon energy	Relative cross sections		
(eV)	Kr $2p_{3/2}$	Kr $2p_{1/2}$	Kr $2s$
1700	1		
1791	0.676	0.324	
1950	0.583	0.283	0.134
13 000	0.298	0.166	0.536

photons of the energies (a) 1709 eV, (b) 1792 eV, (c) 1950 eV, and (d) 13 keV. Due to the selected photon energies panel (a) shows only the L_3-shell Auger decays and panel (b) only the Auger decays of the L_2 and L_3 shells. In contrast to this, panels (c) and (d) show all three L-shell Auger decays. The spectra in panels (a) to (c) overlap with the $4p$, $4s$, $3d$, $3p$, and $3s$ photoelectron lines indicated in green. In addition, also photoelectron satellites, i.e., processes where the ionization is accompanied by an excitation of a valence electron to an unoccupied Rydberg level (e.g., $4p \rightarrow 5p$), can be observed. These transitions are indicated with "s" and cause also satellites in the Auger spectrum; see below.

The advantage of the present approach of using different well-selected photon energies can be seen, e.g., using the weak $L_3M_1M_{4,5}$ transitions as an example. These transitions can readily be identified in the pure L_3 Auger spectrum shown in panel (a). In spectra measured at higher photon energies, see panel (b), these transitions are superimposed by the much more intense $L_2M_{2,3}M_{2,3}$ transitions; for more details, see further below. Moreover, the broader kinetic energy range and improved signal-to-noise ratio compared to previous publications [16–18] allow resolving previously unobserved transitions such as $L_{2,3}M_{4,5}N_{2,3}$ or $L_1M_{4,5}M_{4,5}$.

Although in (c) the photon energy is high enough to ionize the L_1 shell, clear signatures of Auger transitions related to the decay of the L_1 core-hole state cannot be observed. In contrast to this, the spectral features of $L_1M_{2,3}M_{4,5}$ and $L_1M_{4,5}M_{4,5}$ decay are clearly visible in panel (d). These observations can be understood based on two facts. First, as can be seen in Table I, the photoionization cross-section ratio changes with photon energy. At 1950 eV the relative $2p$ ionization cross section is about 6.5 times larger than the $2s$ cross section whereas at 13 keV this ratio is about 1; i.e., the relative contributions of the L_1 Auger decay increase significantly with the photon energy. Second, as recently discussed in Ref. [10], the main Auger channels of the L_1 core-hole state are the Coster-Kronig decays to the L_2 and L_3 holes; these Auger decays are at much lower energies (4–223 eV; see above) and not visible in the present spectra. According to the present calculations, the L_1 hole decays by about 90% via these Coster-Kronig processes, which leads to two consequences. First, this leads to a much larger lifetime broadening for the L_1 hole ($\Gamma(L_1)_{\text{theo}} = 4.28$ eV [37]) as compared to the L_2 ($\Gamma(L_2)_{\text{theo}} = 1.31$ eV [37]) and L_3 ($\Gamma(L_3)_{\text{theo}} = 1.17$ eV [37], $\Gamma(L_3)_{\text{exp}} = 1.152(20)$ eV [38]) holes and results in significantly larger widths for the $L_1M_{2,3}M_{4,5}$ and $L_1M_{4,5}M_{4,5}$ transitions as compared to the L_2 and L_3 Auger decays, and as a consequence to much lower peak intensities. Second,
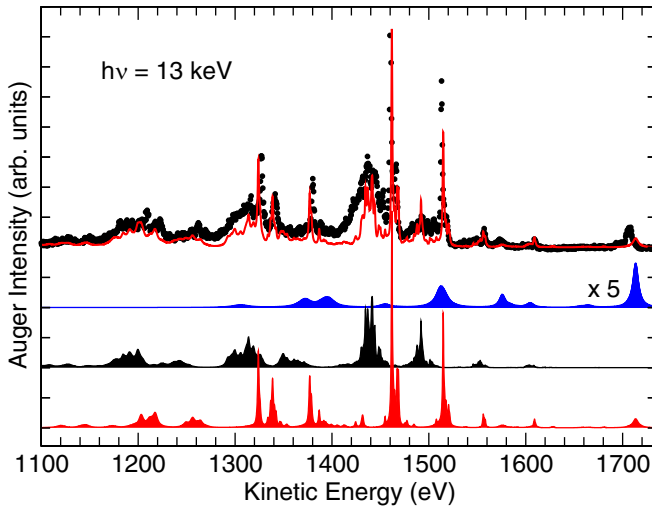
FIG. 2. Experimental (data points) and theoretical (red curve through data points) data for ionization with a photon energy of 13 keV. The red and black subspectra show the contributions of the *LMM* Auger decay of the Kr$^+$ ions and the $L_{2,3}Y$-XXY Auger decays of Kr^{2+} ions formed by Coster-Kronig decay, respectively. For the blue subspectrum showing only the L_1MM Auger decays of Kr$^+$ the intensities are multiplied by 5.

the differences of the spectra shown in panels (c) and (d) of Fig. 1 can be explained by the Auger decays of the Kr^{2+} ions produced by the Coster-Kronig Auger decay of the L_1 core hole; see black subspectrum in Fig. 2. These Kr^{2+} contributions amount at 13 keV almost to 50% of the Auger intensity. This can be understood by the fact that at 13 keV the L_1 hole possesses a relative cross section of almost 54% and decays by about 90% via the Coster-Kronig process.

The agreement of the red theoretical curve and the data points in the upper panel of Fig. 2 is generally very good. Small deviations are due to shake-up satellites in the Auger decay, which are not taken into account in the present calculations.

A. The *LMM* Auger transitions in Kr$^+$

In Figs. 3 to 6 details of the *LMM* Auger transitions of Kr$^+$ are shown. The spectra are aligned along the binding energy of the two-hole states of the main group of the spectrum which is shown on the uppermost axis of each figure. The two-hole binding energy is determined by the kinetic energy of the L_3 Auger transitions and a L_3 ionization energy of 1679.154(91) eV obtained from the energy splitting of the L_3 and N_3 level [38] and the N_3 ionization energy [39]. For an alignment to the two-hole binding energy the kinetic energies of the L_2 spectrum [panels (b)] and the L_1 spectrum [panels (c)] are higher by 52.6(1) and 246.3(6) eV, respectively. In principle, these shifts correspond to the differences of the ionization energies of the L_3 and L_2 (L_1) thresholds. The splitting between the L_3 and L_1 scatters in the literature between 241.61(33) eV and 246.4(1.4) eV, i.e., by almost 5 eV; see Refs. [40,41] and references therein. In contrast to this, the values for the splittings between the L_2 and L_3 thresholds reported in the literature are all between 52.4 and 52.7 eV.
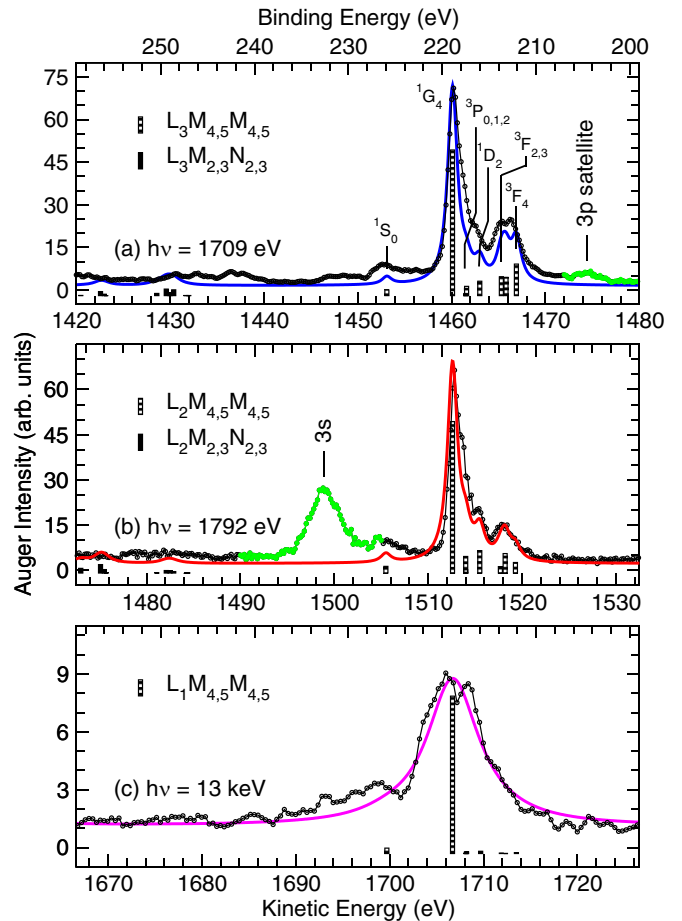

FIG. 3. The $L_3M_{4,5}M_{4,5}$ (a), the $L_2M_{4,5}M_{4,5}$ (b), and the $L_1M_{4,5}M_{4,5}$ Auger transitions (c), which are aligned along the two-hole binding energy; see upper axis. The theoretical energy positions and Auger rates are indicated by the lower vertical bars and the calculated spectra of the L_3, L_2, and L_1 transitions by the blue, red, and magenta solid subspectra, respectively. The spectra also exhibit minor Auger transitions as well as photoelectron lines which are discussed in detail in the text. For reasons of presentation the experimental spectra in panels (a) and (c) are averaged over three data points.

Because of the large differences reported in the literature for the splitting between the thresholds L_3 and L_1, we fitted the $LM_{4,5}M_{4,5}$ Auger transitions in order to derive an additional value from the differences in the kinetic energies of the Auger electrons. These fits resulted in a splitting of 52.6(1) eV between L_3 and L_2 as well as 246.3(6) eV between L_3 and L_1. The present data are in line with the larger splittings between L_1 and L_3 reported in the literature, and in particular with the value of 245.4(8) eV suggested in the critical review by Vénos *et al.* [41].

Figure 3 displays the different $LM_{4,5}M_{4,5}$ Auger transitions. The dashed black vertical bars indicate the calculated energy positions and Auger rates of these transitions. In addition, the filled black vertical bars above 247 eV binding energy in panels (a) and (b) display the theoretical results for the $L_{2,3}M_{2,3}N_{2,3}$ Auger transitions. Note that details for the transitions represented by vertical bars in the Figs. 3 to

6 including the assignment can be found in Table 1 of the Supplemental Material [42].

Although the present calculations are performed using jj coupling, the $L_3M_{4,5}M_{4,5}$ Auger transitions are labeled in the upper panel using the Russell-Saunders coupling scheme $^{2S+1}L_J$, in agreement with previous works [17–19]. The splitting between the states with different total angular momentum L is larger than the spin-orbit splitting of the triplet states indicating that the Russell-Saunders coupling describes these states quite well. However, according to the present calculations and the calculations of Levin *et al.* [18], the splitting between the different ^3F_J states does not strictly obey the Landé interval rule. This indicates that the LS coupling is not strictly valid for these states.

For most of the intense group of transitions the LS coupling is the best description of the final states. For the $M_{2,3}M_{2,3}$ final states the strongest spin-orbit interaction can be expected. Nevertheless, the leading jj contribution to the final states shows coefficients of $|c_i|^2 \cong 0.84$. This is between $2/3$ for pure LS coupling [e.g., $np^{-2}(^1S_0) = \sqrt{\frac{2}{3}}|\frac{3}{2}\frac{3}{2}\rangle_0 + \sqrt{\frac{1}{3}}|\frac{1}{2}\frac{1}{2}\rangle_0$] and 1 for pure jj coupling, and shows that for this configuration an intermediate coupling can be assumed. On the other hand, a pure $|jj\rangle_J$ state has at least a leading contribution of $2/3$ for one $^{2S+1}L_J$ state so that even in this extreme case an assignment based on this coupling is still meaningful. Nevertheless, we want to point out that the final states $M_{2,3}N_1$ are close to pure jj states and the final states $M_{2,3}N_{2,3}$ are probably described best by the jK coupling scheme; however, the transitions to these states are very weak and not unambiguously observed.

The solid colored lines represent the theoretical spectra and are obtained by convoluting the vertical bars with a Lorentzian. The width of each Lorentzian is the sum on the calculated lifetime broadenings of the initial and final state of each transition. The theoretical spectra of the L_3 transitions (red subspectrum), the L_2 transitions (blue subspectrum), and the L_1 transitions (magenta subspectrum) are shifted by 1.5 eV, 2.2 eV, and 6.7 eV to lower energies. These different shifts are due to different deviations between the experimental and the theoretical thresholds ($L_{3,\text{theo}} = 1678.90$ eV, $L_{2,\text{theo}} = 1731.90$ eV, and $L_{1,\text{theo}} = 1930.4$ eV).

At binding energies above 246 eV, in the theoretical spectra of the L_3 and L_2 decays, see panels (a) and (b), the transitions to the $M_{2,3}N_{2,3}$ final states can be observed. These transitions can be separated into two groups with a splitting identical to the splitting of the $3p_j$ states; i.e., they can be described by jK coupling as discussed above. These transitions are possibly present also in the experimental spectra. However, they cannot be clearly identified, although there are several weak structures in the binding energy region from 240 to 260 eV since in this region also the shake-up transitions during the Auger decay of the type $4p^6 \rightarrow 4p^5np$ are expected. In particular, the strongest $4p^6 \rightarrow 4p^55p$ shake-up transitions are expected, based on the corresponding excitation energies of the $Z + 2$ atom Sr III about 28 eV [39] above the binding energy of the corresponding diagram line. Such shake-up transitions during the Auger decay have been observed in the Ar KLL [14] and the Xe $L_{2,3}M_{4,5}N_{4,5}$ [31] Auger spectra.
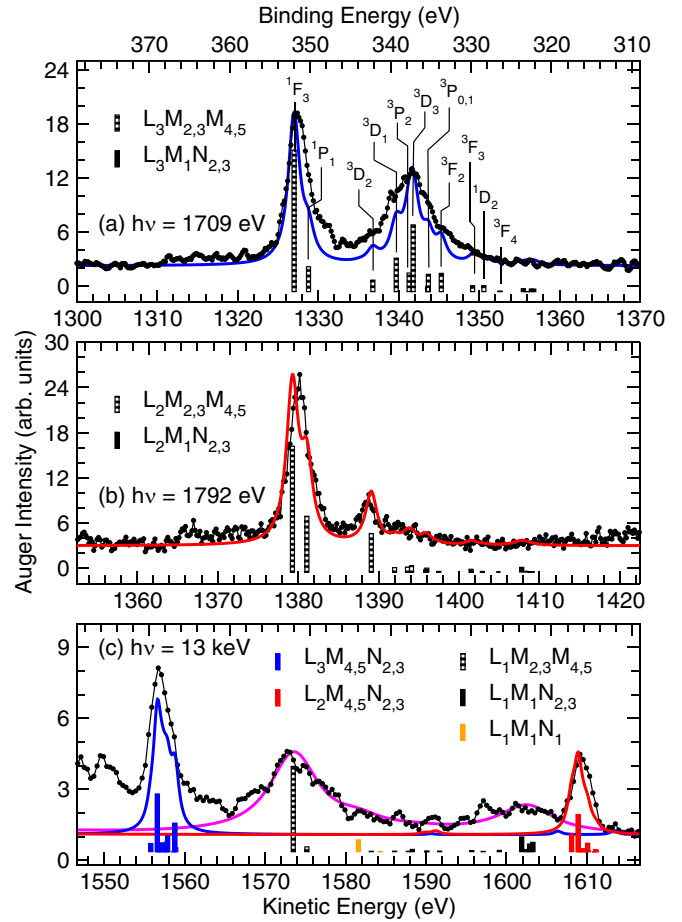

FIG. 4. The $L_3M_{2,3}M_{4,5}$ (a), the $L_2M_{2,3}M_{4,5}$ (b), and the $L_1M_{2,3}M_{4,5}$ Auger transitions (c), which are aligned along the two-hole binding energy; see upper axis. The theoretical energy positions and Auger rates are indicated by the lower vertical bars and the calculated spectra of the L_3, L_2, and L_1 transitions by the blue, red, and magenta solid subspectra, respectively. The spectra also exhibit minor Auger transitions which are discussed in the text. For reasons of presentation the experimental spectra in panels (a) and (c) are averaged over three data points.

In the binding-energy region of $\cong 222$ to 234 eV of the L_3 decays there is also some intensity which is not reproduced by theory. These spectral features can be assigned to the Auger decays of shake-up states during the photoionization process, which are expected to be much closer to the main line than the shake satellites originating during the Auger decay [14,15]. This is in line with the discussion of the Auger decay of the $2p_{3/2}^{-1}4(s, p)^{-1}$ states as will be discussed further below; see Fig. 8. The spectrum shown in Fig. 3 is, however, measured only 30 eV above the L_3 threshold, so that shake satellites are not fully developed. In the L_2 spectrum this energy region around 235 eV is dominated by the strong and broad direct $3s^{-1}$ photoelectron line.

Figure 4 shows the Auger spectra in the binding-energy region from 309 to 370 eV which is dominated by the $LM_{2,3}M_{4,5}$ transitions. In addition, the $LM_1M_{2,3}$, the $L_{2,3}M_{4,5}N_{2,3}$, and the $L_1M_1N_1$ transitions contribute to the spectra. The theoretical L_3 spectra in panels (a) and (c) are shifted by 3 eV to higher

kinetic energies and 0.5 eV to lower kinetic energies, respectively, in order to match well the experimental $L_3M_{2,3}M_{4,5}$ and $L_3M_{4,5}N_{2,3}$ transitions. The L_2 and L_1 spectra are shifted accordingly. The different shifts account for inaccuracies in the calculation of Auger energies. In the upper panel (a) these transitions are assigned using the LS coupling scheme, although the energetic order of the states and the splitting of the triplet states into the different J levels deviate strongly from what is expected in the case of a strict Russell-Saunders coupling scheme, so that an intermediate coupling has to be assumed. However, the observed sequence of energy positions for the different $M_{4,5}N_{2,3}$ final states matches much better the expectation for this configuration in LS coupling than in jj coupling, as discussed by Cowan in his book [43].

It is known from the literature that the Kr $3p^{-1}$ levels interact strongly with the $3d^{-2}nl$ configurations [44], leading to a complex photoelectron spectrum with more than two spin-orbit-split lines. These correlation effects are not taken into account in the present calculations, which are marked for the $L_3M_{2,3}M_{4,5}$ and $L_2M_{2,3}M_{4,5}$ transitions by blue and red solid lines, respectively. Nevertheless, a good agreement between experiment and theory is observed, indicating that the present calculations reproduce the essential part of the physics involved. The $LM_{2,3}M_{4,5}$ transitions can be divided into two groups which are separated by $\cong 15$ eV. The intensity of the states belonging to the group of final states with lower binding energies decreases significantly from the L_3 threshold in panel (a) to the L_1 threshold in panel (c). Because of this, the various Auger spectra look rather different.

At binding energies around 345 eV and from 358 to 370 eV $L_3M_{2,3}M_{4,5}$ [panel (a)] and $L_2M_{2,3}M_{4,5}$ Auger intensities [panel (b)] can be found, which are not reproduced by theory. These spectral features can be assigned to satellite transitions. In detail, the satellites around 345 eV, which are seen only in panel (a), are probably caused by the Auger decay of photoelectron satellites; this assignment is based upon the energy splitting relative to the Auger transitions around 337 eV binding energy. Note that the L_3 spectrum is measured using a photon energy which is $\cong 30$ eV higher than the corresponding ionization energy, so that $2p_{3/2}^{-1}4p^{-1}np$ final states can energetically be populated. The structures between 358 and 370 eV binding energy can be assigned to satellite transitions during the Auger decay, since in the case of L_2 ionization the used photon energy of 1750 eV is only by $\cong$ 18 eV above the L_2 ionization energy and below the ionization energy of the corresponding photoelectron satellites; see also Fig. 7 below.

In the lowest panel (c) the magenta curve representing the L_1 Auger decays agrees well with the experimental spectrum in the binding energy range from 320 to 365 eV, corresponding to $L_1M_1N_1$ and $L_1M_1N_{2,3}$ Auger transitions. These transitions are much stronger in the L_1 Auger spectrum than in the $L_{2,3}$ Auger spectra. This can be explained with a better overlap of the M_1 shell with the L_1 shell than with the $L_{2,3}$ shells, due to the angular distribution of the involved orbitals. Finally, panel (c) also shows the weak $L_{2,3}M_{4,5}N_{2,3}$ Auger transitions.

Figure 5 displays the $L_3M_{2,3}M_{2,3}$ and the $L_2M_{2,3}M_{2,3}$ Auger transitions. In this and the next figure the L_1 spectra
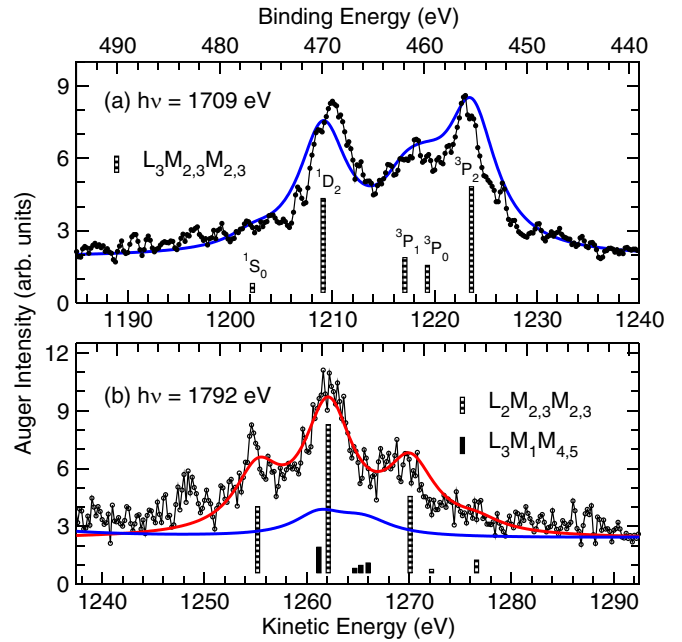

FIG. 5. The $L_3M_{2,3}M_{2,3}$ (a) and the $L_2M_{2,3}M_{2,3}$ (b) Auger transitions, which are aligned along the two-hole binding energy; see upper axis. The theoretical energy positions and Auger rates are indicated by the lower vertical bars and the calculated spectra of the L_3 and L_2 transitions by the blue and red solid subspectra, respectively. The spectrum in (b) also exhibit minor Auger transitions. For reasons of presentation the experimental spectrum in panel (a) is averaged over three data points.

are not displayed, since the corresponding transitions are very weak, see Fig. 2, and are superimposed by stronger transitions. As discussed above, the interaction which causes the spitting between the $M_{2,3}M_{2,3}$ final states is described best by an intermediate coupling. The $L_2M_{2,3}M_{2,3}$ Auger transitions in the lower panel overlap with the $L_3M_1M_{4,5}$ transitions, which will be discussed further below. In the lower spectrum at 1248 eV kinetic energy, Auger intensity can be found which is not reproduced by theory, and it shows no counterpart in the $L_3M_{2,3}M_{2,3}$ Auger spectrum. Based on the used photon energy of 1750 eV, the Auger decay of a photoelectron satellite can be excluded. A satellite caused by a shake-up during the Auger decay is expected at at least 28 eV above the corresponding main line; however, no strong main line can be observed at kinetic energies of 1276 eV or higher. Since no explanation of this line as an Auger satellite is possible, we assign it as an L_3N-MMN Auger decay of Kr^{2+}, which is a result of a Coster-Kronig decay of Kr$^+$ with a hole in the L_2 shell, i.e., by the process Kr $2p_{1/2}^{-1} \rightarrow 2p_{3/2}^{-1}4(s, p)^{-1} + e^-$. We shall discuss these contributions in more detail further below. Note that the present calculations predict the $L_3N_{1,2,3} \rightarrow M_1M_{4,5}N_{1,2,3}$ transitions exactly at this energy position.

The weak $L_3M_1M_{2,3}$ (a), $L_2M_1M_{2,3}$ (b), $L_3M_1M_{4,5}$ (c), and $L_2M_1M_{4,5}$ (d) Auger transitions can be seen in Fig. 6. The spectral features in this figure are very broad since the short-lived M_1 core hole is part of the final states; note that this hole can relax via super-Coster-Kronig decay to $M_{4,5}M_{4,5}$. The intensities and the energy positions of the $L_3M_1M_{2,3}$ Auger transitions agree reasonably well with the results of
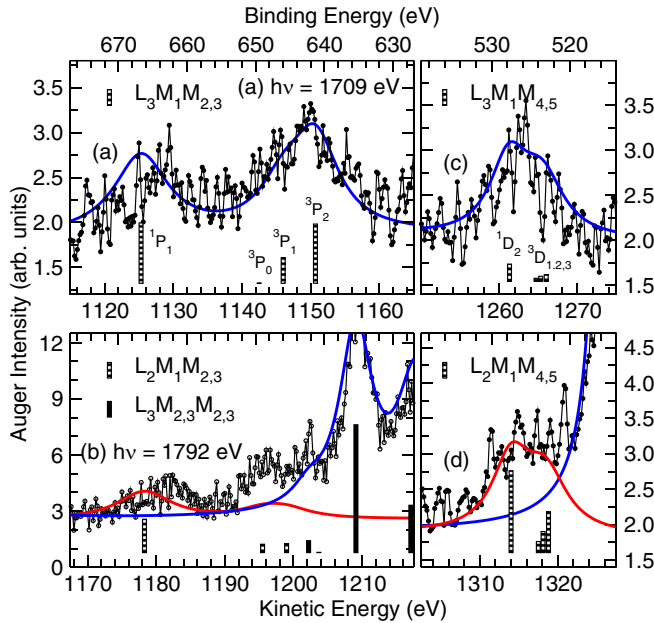
FIG. 6. The $L_3M_1M_{2,3}$ (a), the $L_2M_1M_{2,3}$ (b), the $L_3M_1M_{4,5}$ (c), and the $L_2M_1M_{4,5}$ (d) Auger transitions which are aligned along the two-hole binding energy; see upper axis. The theoretical energy positions and Auger rates are indicated by the lower vertical bars and the calculated spectra of the L_3 and L_2 transitions by the blue and red solid subspectra, respectively. The spectra in (b) and (d) also exhibit strong Auger transitions of the L_3 threshold. For reasons of presentation the experimental spectra in panels (a) and (c) are averaged over three data points.

Lewin *et al.* [18]. The other transitions were not reported in previous publications. For both groups of final states the splitting is very close to the expectation based on *LS* coupling. Furthermore, the $L_2M_1M_{2,3}$ transitions almost overlap with the $L_3M_{2,3}M_{2,3}$ transitions. In particular at the energy position of the $L_2M_1M_{2,3}$ transitions significant satellite contributions of the $L_3M_{2,3}M_{2,3}$ transitions can be expected. In panel (b) at a kinetic energy of $\cong 1195$ eV once again a spectral feature is visible which is not reproduced by the presented theoretical results; note that the calculated $L_2M_1M_{2,3}$ Auger transitions also present in this region are too weak to explain this feature. Because of this, the feature is also assigned to an L_3MM Auger decay of Kr^{2+} and is caused by Coster-Kronig Auger decay of the L_2 hole, namely to $L_3N_{1,2,3} \rightarrow M_{23}M_{23}N_{1,2,3}$. Details will be discussed further below.

B. The $L_{2,3}Y$-MMY Auger decays of Kr^{2+}

In the following we shall discuss the $L_{2,3}Y$-MMY Auger decays of Kr^{2+}. The initial states of these decays can be populated via two different processes, namely first by the Coster-Kronig decays after L_2 and in particular L_1 ionization, and second by the direct L_3 and L_2 ionization accompanied by a shake-off process. Their population via Coster-Kronig decay after L_2 and L_1 ionization is shown in Fig. 7. We would like to remind the reader that the kinetic energies of the Coster-Kronig decays are all below 225 eV and not visible in the present spectra. As displayed in the figure, an L_2 ionization leads only to a Coster-Kronig decay to $L_3N_{1,2,3}$ initial
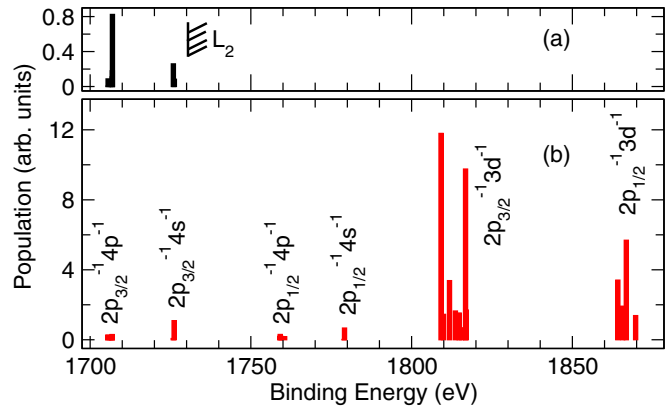

FIG. 7. Population of the different $L_{2,3}N_{1,2,3}$ and $L_{2,3}M_{4,5}$ levels of Kr^{2+} as result of the Coster-Kronig decays after (a) L_2 and (b) L_3 ionization. On the abscissa the binding energy of these states is given.

states. In the case of L_1 ionization and Coster-Kronig decay, $L_{2,3}N_{1,2,3}$ and in particular $L_{2,3}M_{4,5}$ initial states are populated. Shake-off processes accompanying the direct ionization lead mainly to the $L_{2,3}N_{1,2,3}$ states but only to a small extent to the $L_{2,3}M_{4,5}$ states; this result is based on observations for the Kr $1s^{-1}$ satellites [45] and the expectation of similar shake probabilities for the Kr $2(s, p)^{-1}$ thresholds. Shake processes as a source of the population of the $L_{2,3}Y$ states in Kr^{2+} are not taken into account in the present calculations, so that their contribution to the experimental Auger spectra are underestimated.

Before discussing the $L_{2,3}Y$-MMY Auger decays of Kr^{2+} in more detail, we shall present some general statements. For the LMM Auger decay of Kr^+ only 3 initial energy levels exist, namely $L_{1,2,3}$, and about 80 XX final levels so that the entire LXX spectrum consists of less than 250 transitions from which a large number are not intense enough to be observed. In contrast to this, for the Auger decays of Kr^{2+} after Coster-Kronig decay of the L_2 (L_1) core hole, 8 (26) initial levels exist, see Fig. 7, and more than 500 XXX final levels. As a result, the $L_{2,3}X$-XXX Auger spectrum after Coster-Kronig decay of an L_2 core hole consists of about 4000 transitions and that of an L_1 core hole about 13 000 ones. These numbers illustrate that individual assignments of the spectral features in the $L_{2,3}X$-XXX Auger spectra are not possible. Instead, we shall only give the configurations involved in the transitions belonging to a spectral feature.

Figure 8 shows the $L_{2,3}MM$ Auger spectrum subsequent to ionization with 1792 eV photons. The red line close to the data points represents the theoretical result for this photon energy. The subspectrum in the middle of the figure represents the calculated contribution caused by the $L_3N_{1,2,3}$ states which are populated via the Coster-Kronig Auger decay of the L_2 core hole. The spectral features of the transition to the final states $M_{2,3}M_{2,3}N_{1,2,3}$, $M_1M_{4,5}N_{1,2,3}$, $M_{2,3}M_{4,5}N_{1,2,3}$, $M_{2,3}M_{2,3}N_{1,2,3}$, and $M_{4,5}M_{4,5}N_{1,2,3}$ match well the spectral features caused by the Auger decay of the L_3 core hole to the corresponding parent states. The contributions of the $L_3N_{2,3}$-$XXN_{2,3}$ and L_3N_1-XXN_1 Auger transition are indicated by blue and red vertical bars in the lower part of the figure. These bars show that both types of transitions contribute with a
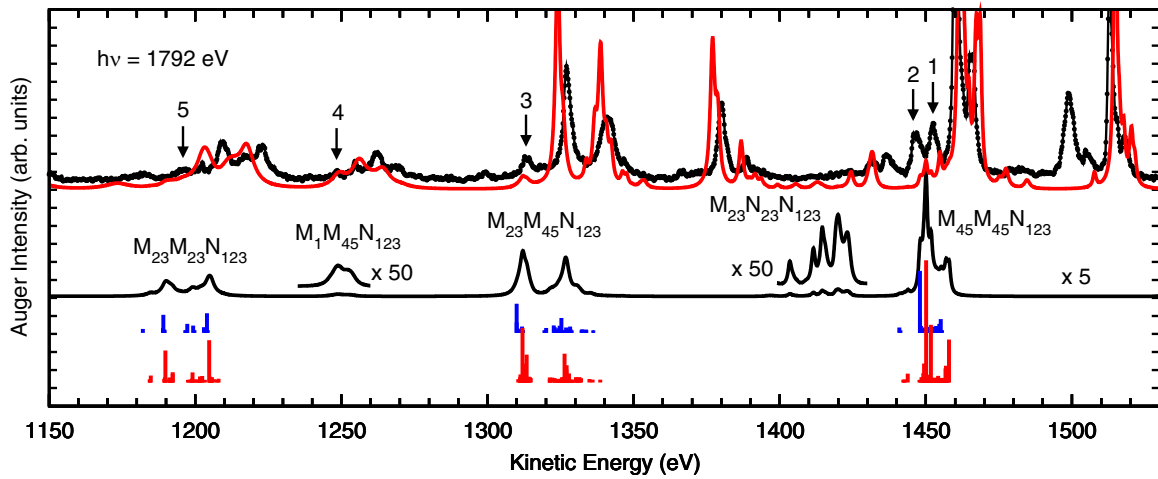
FIG. 8. The data points in the upper part represent the $L_{2,3}MM$ Auger spectrum measured using $h\nu = 1792$ eV. The solid red line close to the data points displays the theoretical result for this photon energy and the solid subspectrum in the middle shows the Auger decays of the $L_3N_{1,2,3}$ states populated via Coster-Kronig decay. The lower red and blue vertical bars indicate the energy positions and intensities of the $L_3N_{2,3}$-$XXN_{2,3}$ and L_3N_1-XXN_1 Auger transitions, respectively.

similar distribution to the spectral feature, with the difference that the L_3N_1-XXN_1 transitions possess on average a kinetic energy which is by $\cong 2$ eV lower than the $L_3N_{2,3}$-$XXN_{2,3}$ transitions. From these findings we conclude that the final states in Kr^{3+} can be described in good approximation by the coupling of the MM parent states $^{2S+1}L_J$, to which the outer hole N_1 or $N_{2,3}$ couples, i.e., $MM(^{2S+1}L_J)N_{123}(^{2S'+1}L'_{J'})$. For the $M_{4,5}N_{2,3}N_{1,2,3}$ final states the situation is obviously more complex since the splitting is not dominated by the interaction between two of the holes.

As stated above, the $L_{2,3}N_1$ and in particular the $L_{2,3}N_{2,3}$ states of Kr^{2+} can also be populated via a shake-off process that accompanies the direct $L_{2,3}$ ionization process. The L_3N_1 and $L_3N_{2,3}$ Auger decays should lead to the same spectral contributions as shown in Fig. 8. However, their additional intensity is not included in the present calculations; i.e., the contributions indicated by the black subspectrum in Fig. 8 represent a lower limit for the $L_3N_{1,2,3}$ Auger decays. Based on the calculations, 5 lines are identified as contributions caused by Coster-Kronig decay or shake-off satellites. Lines 1 and 2 are due to $L_3N_{1,2,3}$-$M_{4,5}M_{4,5}N_{1,2,3}$ Auger transitions, although line 1 possesses in addition contributions of the $L_3M_{4,5}M_{4,5}$ Auger decay to the final state $^1S_0$; see also Fig. 3. Line 3 probably shows two contributions, namely the $L_2M_1M_{4,5}$ Auger decays of Kr$^+$ and the $L_3N_{1,2,3}$-$M_{2,3}M_{4,5}N_{1,2,3}$ Auger transitions of Kr^{2+}. Finally, lines 4 and 5 show contributions which cannot be explained with Auger decays of Kr$^+$, see Fig. 4 as well as Fig. 6 and discussion above. These lines are assigned to the $L_3N_{1,2,3}$-$M_1M_{4,5}N_{1,2,3}$ and $L_3N_{1,2,3}$-$M_{2,3}M_{2,3}N_{1,2,3}$ Auger transitions, respectively. Note that all these spectral features are not visible in the L_3 Auger spectrum measured at 1709 eV. We expect that this energy value is too low to observe fully developed shake-off satellites. Finally, we want to mention that for Ar the $1s^{-1}3p^{-1} \rightarrow 2p^{-2}3p^{-1}$ Auger transitions of the dication overlap with the $1s^{-1}3p^{-1}np \rightarrow 2p^{-2}3p^{-1}mp$ transitions of the cation [14]. We expect a similar behavior for krypton, i.e., contributions

of the Auger decays of the $2p_{3/2}^{-1}4(s, p)^{-1}n(s, p)$ states in the region of peaks 1 to 5. However, a detailed investigation of such contributions is beyond the scope of this publication.

The photon energy of 1792 eV is also too low to produce shake-off satellites of the L_2 threshold; see spectrum in Fig. 1(b). However, the decay of such satellite states can contribute to the spectrum measured at 1950 eV and shown in Fig. 1(c). Actually a detailed comparison of panels (b) and (c) indicates 4 peaks which can be identified based on the present calculations as Auger decays of such satellites. They are indicated in Fig. 1(c) by the numbers 1 to 4. Peaks 1 and 2 are assigned as $L_2N_{1,2,3}$-$M_{4,5}M_{4,5}N_{1,2,3}$ Auger decays. Moreover peaks 3 and 4 are identified as $L_2N_{1,2,3}$-$M_{2,3}M_{4,5}N_{1,2,3}$ and $L_2N_{1,2,3}$-$M_1M_{4,5}N_{1,2,3}$ Auger transitions, respectively. As for the $L_3N_{1,2,3}$ decays, in the region of peaks 1 to 4 contributions of the Auger decays of the $2p_{1/2}^{-1}4(s, p)^{-1}n(s, p)$ states are expected. Note that at the given photon energy the initial states $L_2N_{1,2,3}$ can also be populated via L_1 photoionization and subsequent Coster-Kronig decay.

Finally, we shall discuss the Auger decay of the $L_{2,3}Y$ states, which are populated via Coster-Kronig decay subsequent to L_1 and L_2 ionization with 13 keV photons and presented in Fig. 9. According to the present calculations, these $L_{2,3}Y$ initial states are populated by about 99% via the Coster-Kronig decay of the L_1 core hole and 1% via the L_2 core hole. The different levels for the bar diagrams indicate the different initial states $L_{2,3}M_{4,5}$, $L_{2,3}N_1$, and $L_{2,3}N_{2,3}$. The differently colored vertical bars indicate the various final-state configurations; note that only the most intense transitions are indicated.

As can be readily understood from Fig. 7, the spectrum is dominated by the Auger decays of the $L_{2,3}M_{4,5}$ states, while the $L_{2,3}N_{1,2,3}$ initial states play only a minor role. The $L_{2,3}M_{4,5}$ states decay to the configurations $M_{4,5}M_{4,5}N_{2,3}$ (violet bars), $M_{4,5}M_{4,5}M_{4,5}$ (black bars), $M_{2,3}M_{4,5}N_{2,3}$ (blue bars), $M_{2,3}M_{4,5}N_1$ (cyan bars), $M_{2,3}M_{4,5}M_{4,5}$ (green bars), $M_1M_{4,5}M_{4,5}$ (yellow bars), $M_{2,3}M_{2,3}M_{4,5}$ (red bars), and
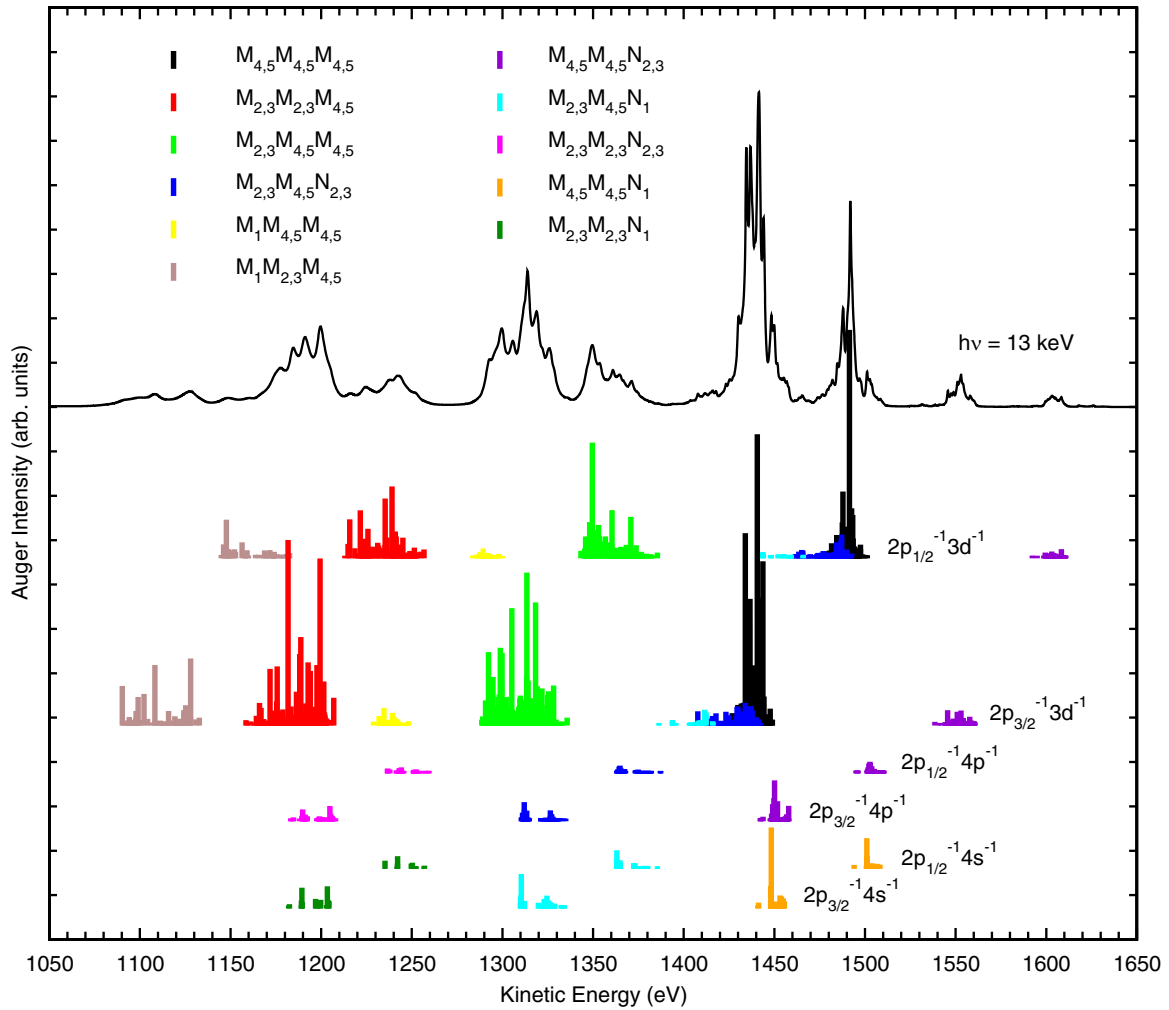
FIG. 9. Upper part: The theoretical $L_{2,3}Y\text{-}XXY$ Auger decays of Kr^{2+} as a result of the Coster-Kronig Auger decays of the L_1 and L_2 holes of Kr^+ subsequent to ionization with 13 keV photons. Lower part: The vertical bar diagrams indicate the main contributions to the spectrum separated according to the different initial states $L_{2,3}Y$ of Kr^{2+}.

$M_1M_{2,3}M_{4,5}$ (brown bars). The states $L_{2,3}N_{2,3}$ decay to the configurations $M_{4,5}M_{4,5}N_{2,3}$, $M_{2,3}M_{4,5}N_{2,3}$, and $M_{2,3}M_{2,3}N_{2,3}$ (magenta bars). Finally, the $L_{2,3}N_1$ states decay to the configurations $M_{4,5}M_{4,5}N_1$ (orange bars), $M_{2,3}M_{4,5}N_1$, and $M_{2,3}M_{2,3}N_1$ (dark green bars). As a result, the final-state configurations $M_{4,5}M_{4,5}N_{2,3}$ and $M_{2,3}M_{4,5}N_1$ are visible in four energy regions, while all other final-state configurations are visible only in two energy regions. The transitions also show that the additional hole in the $M_{4,5}$ or $N_{1,2,3}$ level of the initial state remains with a high probability in that level even after the Auger decay; i.e., it has the function of a spectator.

As already discussed above, the spectral shape of the $L_{2,3}N_{2,3}\text{-}MMN_{2,3}$ and $L_{2,3}N_1\text{-}MMN_1$ transitions match well those of the $L_{2,3}$ transitions of the parent states MM. In contrast to this, the $L_{2,3}M_{4,5}\text{-}MM_{4,5}N_{2,3}$ transitions are spread over an approximately two times larger energy range than the parent states. This can readily be explained with a larger energy spread of the $L_{2,3}M_{4,5}$ initial states as compared to the $L_{2,3}N_{2,3}$ and $L_{2,3}N_1$ initial states; see Fig. 7. The $L_{2,3}M_{4,5}\text{-}MMM_{4,5}$ transitions are spread over an even larger energy range. This can be explained by a stronger interaction

of the $M_{4,5}$ hole already present in the initial state and the two additional MM holes formed during the Auger decay due to the larger spatial overlap of the orbitals.

In the context of the $L_3N_{1,2,3}\text{-}MMN_{1,2,3}$ transitions, we already pointed out that the $L_3N_1\text{-}MMN_1$ transitions are shifted on average by about 2 eV to lower kinetic energies than the $L_3N_{2,3}\text{-}MMN_{2,3}$ transitions. This obviously also holds for the $L_2N_{1,2,3}\text{-}MMN_{1,2,3}$ transitions. In contrast to this, the $L_{2,3}M_{4,5}\text{-}MMN_1$ transitions exhibit about 23 eV lower kinetic energies than the $L_{2,3}M_{4,5}\text{-}MMN_{2,3}$ transitions. This is due to the larger ionization energy of an electron from the N_1 shell than from the $N_{2,3}$ shell since these processes can be considered in good approximation as an $L_{2,3}MN_1$ or $L_{2,3}MN_{2,3}$ Auger decay in the presence of an additional $M_{4,5}$ hole. In contrast to this, the $L_{2,3}N_{1,2,3}\text{-}MMN_{1,2,3}$ transitions can be considered as $L_{2,3}MM$ Auger processes in the presence of an N_1 or $N_{2,3}$ hole which only has spectator character and, therefore, small influence on the Auger energy. Finally, the transitions to the final-state configurations $M_1M_{2,3}M_{4,5}$ and $M_1M_{4,5}M_{4,5}$ are hardly visible in the spectrum, although the calculated intensities are rather larger. However, due to the large lifetime broadening of the M_1 hole of $\cong 3.5$ eV as

estimated from the photoelectron line visible in Figs. 1(a) and 1(b) these transitions are strongly smeared out.

IV. SUMMARY AND CONCLUSION

We present *LMM* Auger spectra of krypton recorded after ionization with photons of $h\nu$ = 1709 eV, 1752 eV, 1950 eV, and 13 keV. The spectrum recorded with the lowest photon energy contains only L_3 Auger decays and the spectrum recorded at $h\nu$ = 1752 eV the L_3 and L_2 Auger decays. The spectra recorded with the two highest photon energies also show contributions of the L_1 Auger decays, however, with different fractions, namely about 13% in the spectrum measured at 1950 eV and about 54% in the spectrum measured at 13 keV. This approach allows recording transitions in addition to those already known from the literature [16–18]. The observed transitions are assigned based on complementary calculations.

The L_2 and the L_1 holes relax by $\cong$ 10% and $\cong$ 90% via Coster-Kronig decay, respectively, and form the states $L_{2,3}N_{1,2,3}$ and $L_{2,3}M_{4,5}$ of Kr^{2+}. Their Auger decays are superimposed with the *LMM* Auger decay of Kr^+ and are also calculated in the present work. It turned out that the spectrum

after L_2 ionization contains about 4000 transitions, while the one after L_1 ionization consists of about 13 000 transitions. The final-state configurations of the most intense transitions are identified and some general properties of the spectral contributions are explained.

The presented Auger decays are due to inner-shell processes, with the expectation of the weak $L_{2,3}N_{1,2,3}$-$MMN_{1,2,3}$ transitions. Because of this, the present results are expected to be similar to the *LMM* Auger spectra of compounds consisting of atoms with similar atomic number Z, such as arsenic, selenium, bromine, rubidium, or strontium. This will allow identifying the spectral features of future high-quality *LMM* Auger spectra which are performed for compounds that consist of these elements.

[1] M. Simon, R. Püttner, T. Marchenko, R. Guillemin, R. K. Kushawaha, L. Journel, G. Goldsztejn, M. N. Piancastelli, J. M. Ablett, J.-P. Rueff, and D. Céolin, Atomic Auger Doppler effects upon emission of fast photoelectrons, Nat. Commun. **5**, 4069 (2014).

[2] D. Céolin, J.-C. Liu, V. Vaz da Cruz, H. Ågren, L. Journel, R. Guillemin, T. Marchenko, R. K. Kushawaha, M. N. Piancastelli, R. Püttner, M. Simon, and F. Gelmukhanov, Recoil-induced ultrafast molecular rotation probed by dynamical rotational Doppler effect, Proc. Natl. Acad. Sci. USA **116**, 4877 (2019).

[3] E. Kukk, T. D. Thomas, D. Céolin, S. Granroth, O. Travnikova, M. Berholts, T. Marchenko, R. Guillemin, L. Journel, I. Ismail, R. Püttner, M. N. Piancastelli, K. Ueda, and M. Simon, Energy Transfer into Molecular Vibrations and Rotations by Recoil in Inner-Shell Photoemission, Phys. Rev. Lett. **121**, 073002 (2018).

[4] M. Kircher, J. Rist, F. Trinter, S. Grundmann, M. Waitz, N. Melzer, I. Vela-Pérez, T. Mletzko, A. Pier, N. Strenger, J. Siebert, R. Janssen, L. Ph. H. Schmidt, A. N. Artemyev, M. S. Schöffler, T. Jahnke, R. Dörner, and P. V. Demekhin, Recoil-Induced Asymmetry of Nondipole Molecular Frame Photoelectron Angular Distributions in the Hard X-ray Regime, Phys. Rev. Lett. **123**, 243201 (2019).

[5] R. Püttner, G. Goldsztejn, D. Céolin, J.-P. Rueff, T. Moreno, R. K. Kushawaha, T. Marchenko, R. Guillemin, L. Journel, D. W. Lindle, M. N. Piancastelli, and M. Simon, Direct Observation of Double-Core-Hole Shake-Up States in Photoemission, Phys. Rev. Lett. **114**, 093001 (2015).

[6] D. Koulentianos, R. Püttner, G. Goldsztejn, T. Marchenko, O. Travnikova, L. Journel, R. Guillemin, D. Céolin, M. N. Piancastelli, M. Simon, and R. Feifel, KL double core hole pre-edge states of HCl, Phys. Chem. Chem. Phys. **20**, 2724 (2018).

[7] G. Goldsztejn, T. Marchenko, R. Püttner, L. Journel, R. Guillemin, S. Carniato, P. Selles, O. Travnikova, D. Céolin, A. F. Lago, R. Feifel, P. Lablanquie, M. N. Piancastelli, F. Penent, and M. Simon, Double-Core-Hole States in Neon: Lifetime, Post-Collision Interaction, and Spectral Assignment, Phys. Rev. Lett. **117**, 133001 (2016).

[8] R. Feifel, J. H. D. Eland, S. Carniato, P. Selles, R. Püttner, D. Koulentianos, T. Marchenko, L. Journel, R. Guillemin, G. Goldsztejn, O. Travnikova, I. Ismail, B. Cunha de Miranda, A. F. Lago, D. Céolin, P. Lablanquie, F. Penent, M. N. Piancastelli, and M. Simon, Cationic double K-hole pre-edge states of CS_2 and SF_6, Sci. Rep. **7**, 13317 (2017).

[9] N. Boudjemia, K. Jänkälä, R. Püttner, T. Marchenko, O. Travnikova, R. Guillemin, L. Journel, I. Ismail, D. Koulentianos, S. Kosugi, Y. Azuma, M. Patanen, M. Huttula, D. Céolin, M. N. Piancastelli, and M. Simon, Electron spectroscopy and dynamics of HBr around the Br $1s^{-1}$ threshold, Phys. Chem. Chem. Phys. **22**, 26806 (2020).

[10] N. Boudjemia, K. Jänkälä, R. Püttner, T. Gejo, L. Journel, Y. Kohmura, M. Huttula, M. N. Piancastelli, M. Simon, and M. Oura, Deep-core photoionization of krypton atoms below and above the *1s* ionization threshold, Phys. Rev. A **101**, 053405 (2020).

[11] N. Boudjemia, K. Jänkälä, T. Gejo, K. Nagaya, K. Tamasaku, M. Huttula, M. N. Piancastelli, M. Simon, and M. Oura, Deep core photoionization of iodine in CH_3I and CF_3I molecules: How deep down does the chemical shift reach?, Phys. Chem. Chem. Phys. **21**, 5448 (2019).

[12] M. N. Piancastelli, K. Jänkälä, L. Journel, T. Gejo, Y. Kohmura, M. Huttula, M. Simon, and M. Oura, X-ray versus Auger emission following Xe *1s* photoionization, Phys. Rev. A **95**, 061402(R) (2017).

[13] M. N. Piancastelli, T. Marchenko, R. Guillemin, L. Journel, O. Travnikova, I. Ismail, and M. Simon, Hard x-ray spectroscopy and dynamics of isolated atoms and molecules: A review, Rep. Prog. Phys. **83**, 016401 (2020).

[14] R. Püttner, P. Holzhey, M. Hrast, M. Žitnik, G. Goldsztejn, T. Marchenko, R. Guillemin, L. Journel, D. Koulentianos, O. Travnikova, M. Zmerli, D. Céolin, Y. Azuma, S. Kosugi, A. F. Lago, M. N. Piancastelli, and M. Simon, Argon *KLL* Auger spectrum: Initial states, core-hole lifetimes, shake, and knockdown processes, Phys. Rev. A **102**, 052832 (2020).

[15] R. Püttner, D. Céolin, R. Guillemin, R. K. Kushawaha, T. Marchenko, L. Journel, M. N. Piancastelli, and M. Simon, Detailed analysis of shake structures in the *KLL* Auger spectrum of H_2S, Phys. Rev. A **93**, 042501 (2016).

[16] L. O. Werme, T. Bergmark, and K. Siegbahn, The high resolution $L_{2,3}MM$ and $M_{4,5}NN$ Auger spectra from krypton and $M_{4,5}NN$ and $N_{4,5}OO$ Auger spectra from xenon, Phys. Scr. **6**, 141 (1972).

[17] H. Aksela, S. Aksela, J. Vayrynen, and T. D. Thomas, $L_{2,3}M_{4,5}X$ Auger electron spectra of Br_2 and Kr: Anomalous $L_2M_{2,3}M_{4,5}$ spectra, Phys. Rev. A **22**, 1116 (1980).

[18] J. C. Levin, S. L. Sorensen, B. Crasemann, M. H. Chen, and G. S. Brown, Krypton *L-MM* Auger spectra: New measurements and analysis, Phys. Rev. A **33**, 968 (1986).

[19] I. H. Suzuki, K. Okada, K. Kamimori, J. Sasaki, H. Yoshida, A. Hiraya, Y. Shimizu, S. Nagaoka, Y. Tamenori, H. Ohashi, and T. Ibuki, Auger electron spectra of Kr $2p$ holes using monochromatic soft x-rays, Surf. Rev. Lett. **9**, 63 (2002).

[20] S. Nagaoka, T. Ibuki, N. Saito, Y. Shimizu, Y. Senba, K. Kamimori, Y. Tamenori, H. Ohashi, and I. H. Suzuki, Resonant Auger spectrum following Kr:$2p \rightarrow 5s$ photoexcitation, J. Phys. B **33**, L605 (2000).

[21] K. Okada, M. Kosugi, A. Fujii, S. Nagaoka, T. Ibuki, S. Samori, Y. Tamenori, H. Ohashi, I. H. Suzuki, and K. Ohno, Variation in resonant Auger yields into the $^1G_4 \cdot nl$ states of Kr across the L_3 threshold, J. Phys. B **38**, 421 (2005).

[22] H. Ohashi, Y. Senba, E. Ishiguro, S. Goto, S. Shin, and T. Ishikawa, Evaluation of modern soft x-ray monochromator with high resolving power over 10000, Proc. SPIE **6317**, 63171A (2006).

[23] H. Ohashi, Y. Senba, H. Kishimoto, T. Miura, E. Ishiguro, T. Takeuchi, M. Oura, K. Shirasawa, T. Tanaka, M. Takeuchi, K. Takeshita, S. Goto, S. Takahashi, H. Aoyagi, M. Sano, Y. Furukawa, T. Ohata, T. Matsushita, Y. Ishizawa, S. Taniguchi *et al.*, Performance of a highly stabilized and high-resolution beamline BL17SU for advanced soft x-ray spectroscopy at SPring-8, AIP Conf. Proc. **879**, 523 (2007).

[24] Y. Senba, H. Ohashi, H. Kishimoto, T. Miura, S. Goto, S. Shin, T. Shintake, and T. Ishikawa, Fundamental techniques for high photon energy stability of a modern soft x-ray beamline, AIP Conf. Proc. **879**, 718 (2007).

[25] T. Mochizuki, Y. Kohmura, A. Awaji, Y. Suzuki, A. Baron, K. Tamasaku, M. Yabashi, H. Yamazaki, and T. Ishikawa, Cryogenic cooling monochromators for the SPring-8 undulator beamlines, Nucl. Instrum. Methods A **467-468**, 647 (2001).

[26] K. Tamasaku, Y. Tanaka, M. Yabashi, H. Yamazaki, N. Kawamura, M. Suzuki, and T. Ishikawa, SPring-8 RIKEN beamline III for coherent x-ray optics, Nucl. Instrum. Methods A **467-468**, 686 (2001).

[27] The analyzer as well as the gas cell were originally supplied by Gammadata Scienta. Present company name is ScientaOmicron.

[28] M. Oura, T. Gejo, K. Nagaya, Y. Kohmura, K. Tamasaku, L. Journel, M. N. Piancastelli, and M. Simon, Hard x-ray photoelectron spectroscopy on heavy atoms and heavy-element containing molecules using synchrotron radiation up to 35 keV at SPring-8 undulator beamlines, New J. Phys. **21**, 043015 (2019).

[29] J. Tulkki, N. M. Kabachnik, and H. Aksela, Effects of channel interaction, exchange, and relaxation on the angular distribution and spin polarization of Auger electrons from noble-gas atoms, Phys. Rev. A **48**, 1277 (1993).

[30] U. Kleiman and B. Lohmann, Photoionization of closed-shell atoms: Hartree-Fock calculations of orientation and alignment, J. Electron. Spectrosc. Relat. Phenom. **131-132**, 29 (2003).

[31] R. Püttner, K. Jänkälä, R. K. Kushawaha, T. Marchenko, G. Goldsztejn, O. Travnikova, R. Guillemin, L. Journel, I. Ismail, B. Cunha de Miranda, A. F. Lago, D. Céolin, M. N. Piancastelli, and M. Simon, Detailed assignment of normal and resonant Auger spectra of Xe near the L edges, Phys. Rev. A **96**, 022501 (2017).

[32] H. Aksela, S. Aksela, and H. Pulkkinen, Correlation effects in $4s^04p^6$ and $4s^14p^5$ configurations of krypton studied by the *MNN* Auger decay, Phys. Rev. A **30**, 2456 (1984).

[33] M. F. Gu, The flexible atomic code, Can. J. Phys. **86**, 675 (2008).

[34] G. Wentzel, Über strahlungslose Quantensprünge, Z. Phys. **43**, 524 (1927).

[35] R. Manne and H. Åberg, Auger transition amplitudes from general many-electron wavefunctions, Chem. Phys. **93**, 201 (1985).

[36] J. Niskanen, K. Jänkälä, M. Huttula, and A. Föhlisch, QED effects in 1s and 2s single and double ionization potentials of the noble gases, J. Chem. Phys. **146**, 144312 (2017).

[37] M. O. Krause and J. H. Oliver, Natural widths of atomic K and L levels, $K\alpha$ x-ray lines and several *KLL* Auger lines, J. Phys. Chem. Ref. Data **8**, 329 (1979).

[38] K. Altenmüller, M. Arenz, W.-J. Baek, M. Beck, A. Beglarian, J. Behrens, T. Bergmann, A. Berlev, U. Besserer, K. Blaum *et al.*, High-resolution spectroscopy of gaseous ^{83m}Kr conversion electrons with the KATRIN experiment, J. Phys. G **47**, 065002 (2020).

[39] Atomic Spectra Database, NIST Standard Reference Database 78, Version 5.8, https://dx.doi.org/10.18434/T4W30F.

[40] O. Dragoun, A. Špalek, and F. J. Wuilleumier, Increased accuracy of the binding energy of K- and L-subshell electrons in krypton from re-analysis of experimental data: Importance for determination of the neutrino mass, Czech. J. Phys. **54**, 833 (2004).

[41] D. Vénos, J. Sentkerestiová, O. Dragoun, M. Slezák, M. Ryšavý, and A. Špalek, Properties of ^{83m}Kr conversion electrons and their use in the KATRIN experiment, J. Instrum. **13**, T02012 (2018).

[42] See Supplemental Material at http://link.aps.org/supplemental/10.1103/PhysRevA.104.012804 for detailed theoretical results. Given are the kinetic energies, intensities of the different Auger transitions, as well as leading configurations and angular momenta J for the states involved in these transitions.

[43] R. C. Cowan, *The Theory of Atomic Structure and Spectra* (University of California Press, Berkeley, 1981), pp. 122.

[44] S. Kosugi, F. Koike, T. Nagayasu, F. Hosseini, J. Martins, T. Marchenko, O. Travnikova, M. Oura, T. Gejo, J. R. Harries, J. D. Bozek, K. Ito, E. Sokell, S. Fritzsche, M. N. Piancastelli, M. Simon, and Y. Azuma, Strong configuration interaction in the *3p* photoelectron spectrum of Kr, Phys. Rev. A **101**, 042505 (2020).

[45] D. L. Wark, R. Bartlett, T. J. Bowles, R. G. H. Robertson, D. S. Sivia, W. Trela, J. F. Wilkerson, G. S. Brown, B. Crasemann, S. L. Sorensen, S. J. Schaphorst, D. A. Knapp, J. Henderson, J. Tulkki, and T. Åberg, Correspondence of Electron Spectra from Photoionization and Nuclear Internal Conversion, Phys. Rev. Lett. **67**, 2291 (1991).